ACS APPLIED MATERIALS & INTERFACES

Letter

www.acsami.org

Dual-Layer-Structured Nickel Hexacyanoferrate/MnO_2 Composite as a High-Energy Supercapacitive Material Based on the Complementarity and Interlayer Concentration Enhancement Effect

Yu Wang[†] and Qianwang Chen*[,†,‡]

[†]Hefei National Laboratory for Physical Sciences at the Microscale, Department of Materials Science & Engineering, Collaborative Innovation Center of Suzhou Nano Science and Technology, University of Science and Technology of China, Hefei 230026, China

[‡]High Magnetic Field Laboratory Hefei Institutes of Physical Science Chinese Academy of Sciences, Hefei 230031, China

Supporting Information

ABSTRACT: A dual-layer composite structure composed of a metal−organic framework structure (NiHCF) with tunable open channels and typical pseudocapacitive manganese dioxide is constructed here as an electrode material for supercapacitors. This type of structure shows enhanced specific capacitance, high energy density, and excellent rate capability and stability. The specific capacitance of the composite electrode is much larger than the sum of each part, and a synergy effect of the dual-layer structure named "interlayer concentration enhancement effect" (ICE effect for short) was proposed to account for this excellent electrochemical performance.

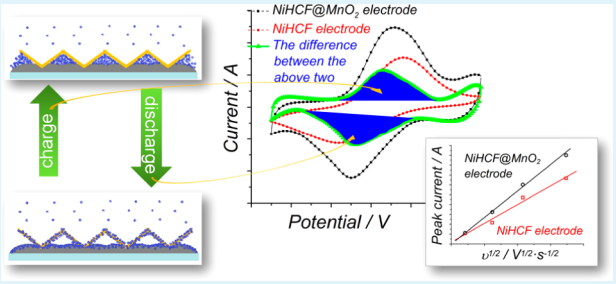

KEYWORDS: *supercapacitors, dual-layer structure, nickel hexacyanoferrate, MnO_2, ICE effect, complementarity*

Capacitors are increasingly becoming one of the most important portable energy storage systems.[1−4] In comparison with batteries, they showed advantages of higher power density, much longer lifespan, no memory effect, better environmental benignity, and lower costs.[1,5] Manganese dioxide (MnO_2)-based materials have been regarded as the most promising cathode materials for supercapacitors because of their capacitor-like electrochemical behavior, excellent reversibility, low cost, good environmental compatibility, and also attractive high specific capacitance (theoretical value is 1300 F g^{-1}),[6,7] which is much higher than that of the currently used active carbon-based cathode (about 150 F g^{-1}).[8] However, because only a very small surface layer of MnO_2 is involved in the charge storage process, their real capacitances and energy densities usually cannot meet the practical demand.[4] Nowadays, many studies on the supercapacitors aim to increase their energy densities as well as decrease fabrication costs.[9−11]

It is impossible to improve the energy density as high as lithium-ion batteries, which originates from the fundamental electrochemical process. Nonetheless, different strategies have been proposed to improve the energy density of MnO_2-based cathodes to the best extent, among which two are widely practiced. One effective protocol is to create designed nanostructured MnO_2 with a high specific surface area. For example, the preconstructed void space provided by hollow or porous structures is the favorite.[12,13] Low-dimensional nanostructures, such as one-dimensional (1D) nanorods/nanowires/nanotubes and two-dimensional (2D) nanosheets, have been tested for electrochemical capacitor applications.[14,15] It was believed that these nanostructures with a large exposed surface and short diffusion length could interact more efficiently with the electrolyte. Another commonly used approach is to introduce a flexible and conductive overlayer, such as carbon nanotubes, graphene, etc., as a physical scaffold to effectively create a new exposed surface and enhance electronic conduction.[15−20] Notwithstanding these advances, the rational design and facile synthesis of MnO_2-based nanostructures for high energy density still remain a challenge. A specific energy of 45 Wh kg^{-1} with a specific capacitance of 937 F g^{-1} was achieved by MnO_2/Mn/MnO_2 sandwich-structured nanotube arrays. However, the specific mass loading was only 0.32 mg cm^{-2}; thus, it cannot provide enough real energy.[15] Moreover, the preparation method is complicated and expensive. In recent years, hybrid systems offer another attractive alternative to improving the energy density by combining a battery-type electrode (energy-density source) with a capacitor-type electrode (power-density source) in the same cell.[1,9,21,22] Although here we prefer to discuss the electrode materials, it is still a very good inspiration that we can construct a composite electrode material composed of a high-energy-storage battery-type material layer and high-power-capacitive MnO_2 layer.

Herein, we propose a novel nickel hexacyanoferrate (NiHCF)/MnO_2 dual-layer composite nanostructure, namely, hierarchical structures constructed of a MnO_2-layer-coated

Received: February 23, 2014
Accepted: May 1, 2014
Published: May 1, 2014

   dx.doi.org/10.1021/am5011173 | ACS Appl. Mater. Interfaces 2014, 6, 6196−6201

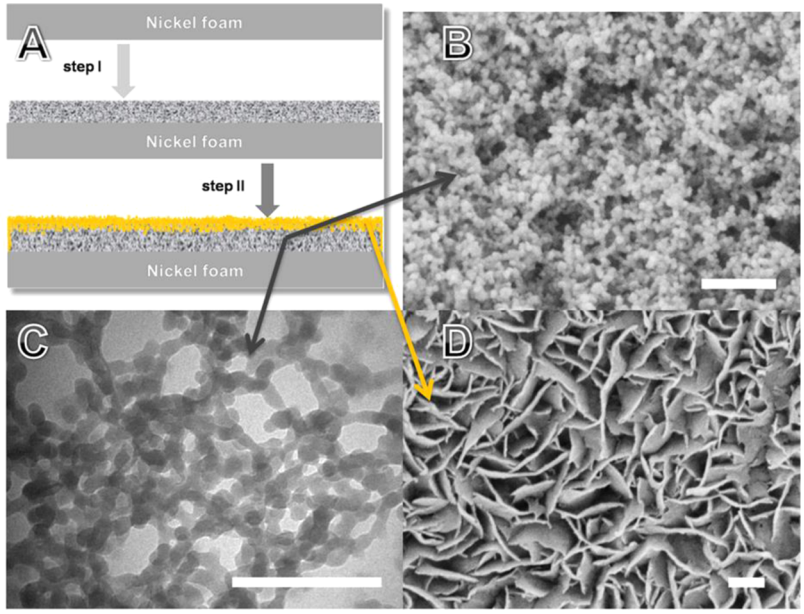

Figure 1. A) Schematic diagram of the strategy for preparing a NiHCF@MnO_2 electrode. (B and D) SEM images of the electrode surface before (B) and after (D) electrodeposition (100 s) of MnO_2. (C) TEM image showing that the NiHCF powders are in nanoscale with diameters below 50 nm and they are interconnected, forming a local-area three-dimensional network. All scale bars are 200 nm.

NiHCF layer (denoted as NiHCF@MnO_2). Metal−organic framework (MOF) structures naturally possess a high surface area because of their tunable open channels and are regarded as good candidates for electrode materials.[23] Recently, Prussian Blue and its analogues have been well-studied in aqueous alkali-metal-ion batteries because of their open spaces, which can accommodate not only neutral molecules but also ions charge-balanced by iron ions, and good performances such as high rate performance, long cycle life, low cost, and a relatively larger energy density were found.[24−26] However, according to our research, its specific capacitance and cycling stability at large scan rates or large current densities, when used as a cathode material for supercapacitors, are yet to be improved. Fortunately, NiHCF is a typical aqueous sodium storage material; together with MnO_2, they share the same mild aqueous electrolyte of Na_2SO_4, and thus the complementary advantages of combination could be realized.

This work aimed at demonstrating the enhanced specific capacitance, high power density, high energy density, and excellent cycling stability of the proposed NiHCF@MnO_2. Through investigating the inner source of those high performances, we proposed a synergy effect of this kind of dual-layer structure and named it the "interlayer concentration enhancement effect" for the first time. The strategy for preparing a NiHCF@MnO_2 electrode is depicted schematically in Figure 1A. In step I, NiHCF, together with acetylene black, are coated on foam nickel (used as the current collector) using poly(vinylidene difluoride) as a binder. In step II, the MnO_2 is anodically electroplated onto the NiHCF electrode. The method of electrodeposition is convenient and frequently used.[27−29] After cleaning and drying, composite NiHCF@MnO_2 electrodes are finally obtained.

NiHCF powders were synthesized through facile coprecipitation. The crystallographic phase of the product is determined by powder X-ray diffraction (XRD), as shown in Figure S1A (Supporting Information, SI). All of the diffraction peaks in the XRD pattern can be unambiguously assigned to an open-framework Prussian Blue hexacyanometalate crystal structure,[30,31] face-centered-cubic $KNiFe(CN)_6$ (JCPDS card no. 51-1897; space group $Fm\bar{3}m$, a = 10.23 Å). TEM images show that the NiHCF powders are in nanoscale with diameters below 50 nm and they are interconnected, forming a local-area three-dimensional network (Figure 1C). The N_2 adsorption−desorption isotherms at 77 K show that NiHCF possesses a large Brunauer−Emmett−Teller (BET) surface area of around 121 $m^2\ g^{-1}$ and a large number of mesopores (Figure S3 in the SI). With relatively high specific surface and appropriate pore-size distribution, the NiHCF can well serve as the framework to support the subsequent electrodeposition of hierarchical MnO_2 nanoplates and also be beneficial to electrolyte infiltration.

Parts B and D of Figure 1 show scanning electron microscopy (SEM) images of the electrode surface before and after electrodeposition of MnO_2; the totally different surface tells us that a layer of MnO_2 has covered the whole electrode. Figure 1D indicates that the MnO_2 layer is composed of randomly oriented thin nanoplates that form a hierarchical architecture. Different deposition times have been investigated (Table S1 and Figure S4 in the SI), and facts have proved that, within a deposition time of 10 s, MnO_2 has already covered the whole electrode and adding deposition time could do nothing but decrease the specific capacitance because only the very surface layer of MnO_2 could get involved in the charge-storage process.[4] The crystallographic phase of the electrode surface is determined by powder XRD, as shown in Figure S1B in the SI; only one peak sticks out and can be assigned to orthorhombic ramsdellite MnO_2, indicating oriented growth and poor crystallization as deposition was performed at room temperature. The X-ray photoelectron spectoscopy (XPS) spectra of Mn 2p and O 1s in the dual-layer structure are shown in Figure S2 in the SI. The binding energy separation (ΔE_{Mn-O}) between the peaks of Mn $2p_{3/2}$ and O 1s [Mn−O−Mn] is 112.3 eV, while the peak of Mn $2p_{3/2}$ is located at 642.2 eV, indicating that MnO_2 has been successfully electrodeposited on the surface of the NiHCF layer.[32]

dx.doi.org/10.1021/am5011173 | ACS Appl. Mater. Interfaces 2014, 6, 6196−6201

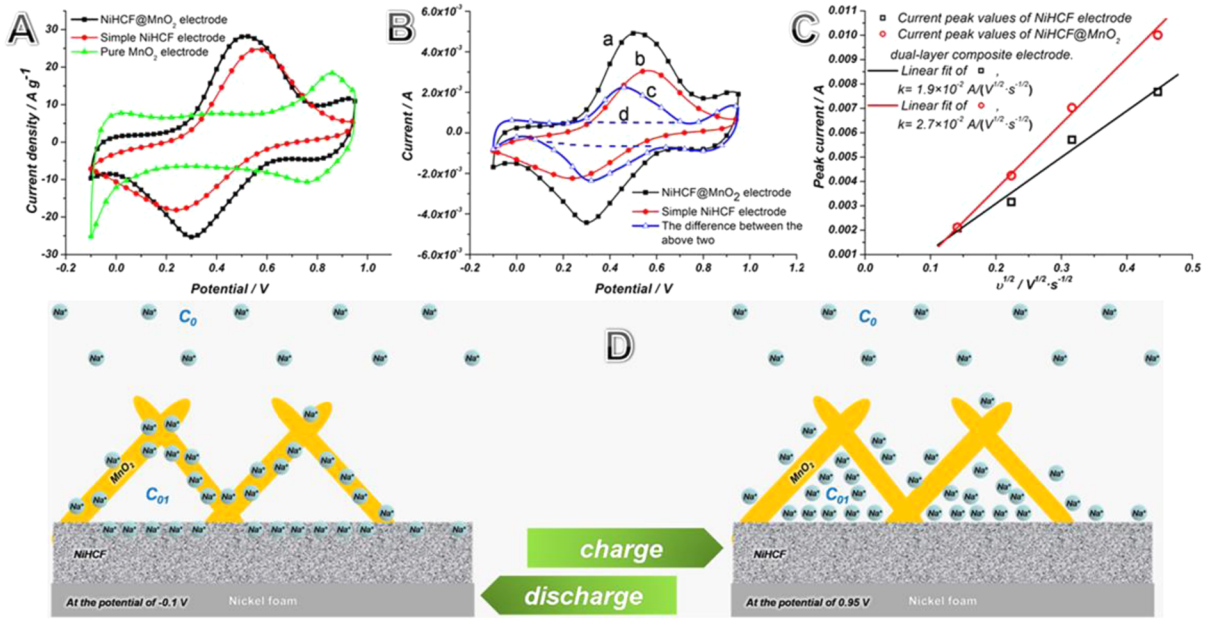

Figure 2. (A) CVs for the three kinds of electrodes (the NiHCF@MnO_2 electrode and the simple NiHCF and pure MnO_2 electrodes) at a scan rate of 50 mV s^{-1} in the voltage window of −0.1 to +0.95 V vs Ag/AgCl. (B) Cyclic voltammetry behaviors of a NiHCF electrode before (b) and after (a) electrodeposition of MnO_2 and the difference between their current valves calculated and plotted as curve c. (C) From the CV curves of both NiHCF and NiHCF@MnO_2 electrode at different scan rates, relationships between the anodic peak current i_p (the current produced by MnO_2 has been deducted) and the square root of the scan rate $v^{1/2}$. (D) Schematic diagram showing the different Na^+ ion concentrations in the space between the NiHCF and MnO_2 layers (C_{01}) at charged (right) and discharged (left) states.

We subsequently investigated the electrochemical properties of NiHCF@MnO_2 as a cathode material for supercapacitors, with the simple NiHCF and pure MnO_2 (also synthesized by electrodeposition) as a comparison. Figure 2A shows the cyclic voltammograms (CVs) for the three kinds of electrodes at a scan rate of 50 mV s^{-1} in the voltage window of −0.1 to +0.95 V vs Ag/AgCl. The quasi-rectangular-shaped cyclic voltammetry curve of the pure MnO_2 electrode, which indicates its pseudocapacitive property, is generally consistent with those of MnO_2 reported in the literature,[1,4,32] suggesting similar electrochemical reaction pathways: the electrochemical capacitance comes from conversion between Mn^{III} and Mn^{IV} accompanied by intercalation and deintercalation of alkali-metal ions. For a NiHCF electrode, the current changed slowly at the beginning of the voltage switching (−0.1 or 0.95 V) and a pair of big redox current peaks rose suddenly between 0.1 and 0.7 V. The anodic peak at about 0.55 V indicated that the Fe^{2+} ions were converted to Fe^{3+} ions and Na^+ ions were unloaded from the electroactive material in the meantime; the cathodic peak at about 0.25 V indicated the reverse process.[24,25,33] For the NiHCF@MnO_2 composite electrode, its cyclic voltammetry curve combined the characteristics of both NiHCF and MnO_2. The nearly vertical line at the beginning of the voltage switching (−0.1 or +0.95 V) and the subsequent big redox current peaks imply integration of both superiorities. Not only that, the specific capacitance of the composite electrode is much larger than the sum of its parts. From these cyclic voltammetry curves, the specific capacitances of the three kinds of electroactive materials were calculated to be 177.5 F g^{-1} for a simple NiHCF electrode, 172 F g^{-1} for a pure MnO_2 electrode, and 224 F g^{-1} for a NiHCF@MnO_2 dual-layer composite electrode at a scan rate of 50 mV s^{-1}. All of the mass loadings were calculated from the results of inductively coupled plasma mass spectrometry. Thus, the excess specific capacitance can be calculated by the formula $C_{s,excess} = C_{s,composite} - 70.5\% \times C_{s,NiHCF} - (1-70.5\%)C_{s,MnO_2}$, where C_s stands for the specific capacitance and the mass percentage of NiHCF in the composite is 70.5%. Where does the excess specific capacitance (=48.2 F g^{-1}) come from?

Figure 2B shows us the cyclic voltammetry behaviors of a NiHCF electrode before (b) and after (a) electrodeposition of MnO_2, and the differences between their current valves were calculated and plotted as curve c. Compare curve c with the cyclic voltammetry curve of pure MnO_2; apparently, in addition to the changeless current of MnO_2 at the potential between 0.1 and 0.7 V, which was designed as curve d, a pair of current peaks unexpectedly occurred. Because the two current peaks do not belong to MnO_2 and the redox current peaks of NiHCF have been deducted and, in addition, no chemical changes happened to NiHCF during the deposition process, which can be known from the XPS spectra (Figure S2A,B in the SI), they were supposed to be derived from the synergy effect of the dual-layer composite nanostructure. That is the reason why the specific capacitance of the dual-layer composite is larger than the sum of its parts. In order to investigate the inner mechanism of the enhanced specific capacitance, the cyclic voltammetry curves of both the NiHCF and NiHCF@MnO_2 electrodes at different scan rates (Figure S5 in the SI) were studied. Also, the relationship between the anodic peak current i_p (the current produced by MnO_2 has been deducted) and the square root of the scan rate $v^{1/2}$ is shown in Figure 2C. The anodic peak current of both electrodes increases linearly with the square root of the scan rate, indicating a mass-transport-controlled process. The slope of the linear fitting was calculated to be $k = 1.9 \times 10^{-2}$ A/($V^{1/2}$·$s^{-1/2}$) for the NiHCF electrode and 2.7×10^{-2} A/($V^{1/2}$·$s^{-1/2}$) for the NiHCF@MnO_2 electrode. At room temperature, the relationship between the peak current (i_p) and the square root of the scan rate ($v^{1/2}$) is

dx.doi.org/10.1021/am5011173 | ACS Appl. Mater. Interfaces 2014, 6, 6196−6201

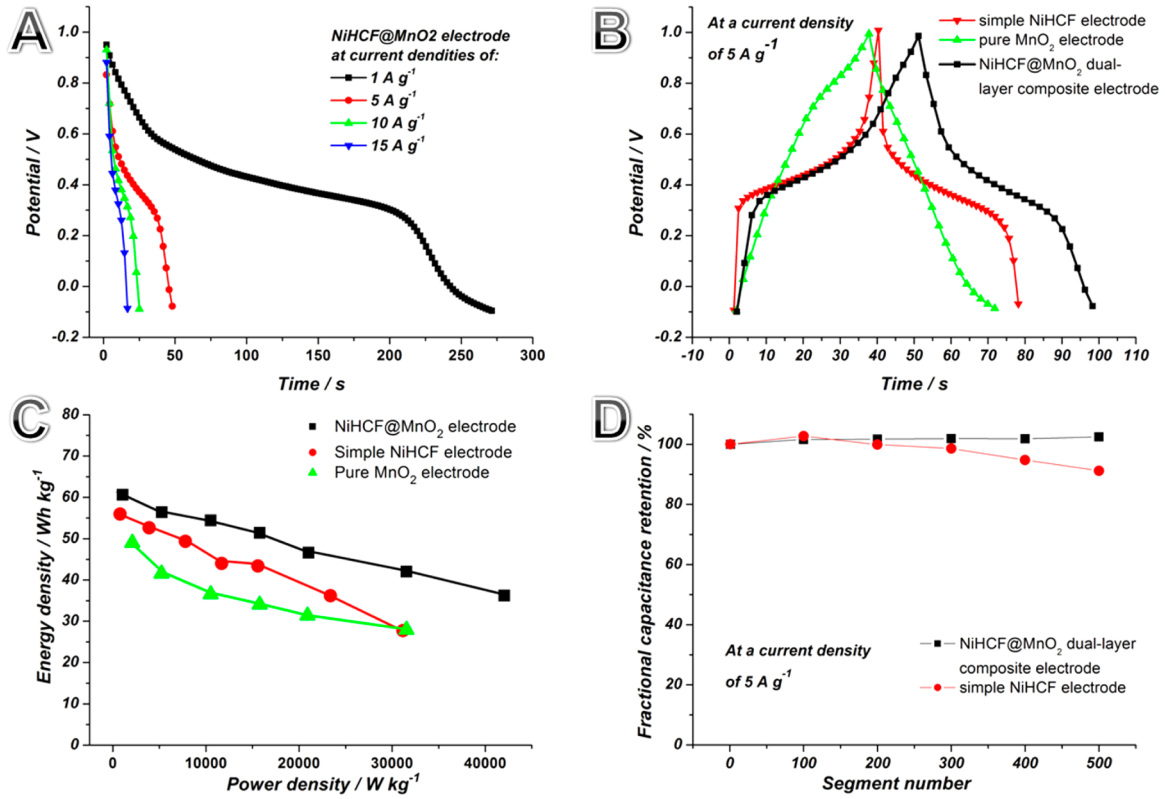

Figure 3. (A) Galvanostatic discharge of the NiHCF@MnO_2 electrode at different current densities carried out between −0.1 and +0.95 V vs Ag/AgCl. (B) Charge/discharge behavior of a simple NiHCF electrode, a pure MnO_2 electrode, and a NiHCF@MnO_2 dual-layer composite electrode evaluated at a current density of 5 A g^{-1}. (C) Energy−power plots of the three kinds of electrodes. (D) Charge/discharge cycling performance evaluated between −0.1 and +0.9 V at a current density of 5 A g^{-1}.

given by the diffusion equation $i_p = 2.69 \times 10^5 An^{3/2}C_0D^{1/2}v^{1/2}$,[34,35] where n is the number of electrons transferred per molecule during the electrochemical process, A is the surface area of the electrode (because NiHCF is a MOF structure, the surface area is huge), C_0 is the concentration of diffusion species (Na^+), D is the diffusion coefficient of Na^+, and v is the potential scan rate. According to the equation above, slope $k = 2.69 \times 10^5 An^{3/2}C_0D^{1/2}$. Among these factors, because n and D remain constant and A might even somewhat decrease after electrodeposition of MnO_2, the larger k of the dual-layer composite electrode can only originate from the larger C_0. At the potential of −0.1 V, both Fe in NiHCF and Mn in MnO_2 were in states of low valence, and the diffusion species (Na^+) were embedded in them; thus, C_{01}, the electrolyte concentration in the space between the NiHCF and MnO_2 layers, is much lower than C_0. That larger electrolyte concentration gradient leads to a larger slope k and also a higher current peak during the charge process. In the reverse process, both Fe in NiHCF and Mn in MnO_2 were in states of high valence, and Na^+ ions apart from both NiHCF and MnO_2 were accumulated in the space between the NiHCF and MnO_2 layers at a potential of 0.95 V; thus, C_{01} is much higher than C_0, as depicted in Figure 2D. Consequently, during the discharge process, the current peak of the dual-layer composite electrode is also higher than that of the simple NiHCF electrode. Because the enhanced capacitance stems from the ion concentration inside the MnO_2 layer, the synergy effect of this kind of dual-layer structure is named an "interlayer concentration enhancement effect", which can be abbreviated as the ICE effect.

During cycling at a scan rate of 20 mV s^{-1}, a capacitance of 240.7 F g^{-1} was observed, and 70.8% of this capacitance, 170.4 F g^{-1}, was retained during cycling at a rate 10 times greater, 200 mV s^{-1}. The high capacitance retention at high scan rates indicates the superiority of rapid charge and discharge, while the capacitance retention is only 62.8% for that of simple NiHCF electrode.

To get more information about the NiHCF@MnO_2 electrode, galvanostatic charge/discharge measurements at different current densities were carried out between −0.1 and +0.95 V (vs Ag/AgCl). Excellent rate capability, superior to that of most reported composite electrodes, is illustrated in Figure 3A; during cycling at a current density of 1 A g^{-1}, a capacitance of 199.6 F g^{-1} was achieved, and 91.6% of this capacitance, 182.8 F g^{-1}, was retained during cycling at a rate 15 times greater, 15 A g^{-1}.[15,16,20,36] Figure 3B shows the charge/discharge behaviors of a simple NiHCF electrode, a pure MnO_2 electrode, and a dual-layer composite electrode evaluated at a current density of 5 A g^{-1}. As expected, an almost linear shape with nearly symmetric charge and discharge curves of a MnO_2 electrode reveals a fast and reversible faradaic reaction.[37] Also, the other two both possess charge/discharge plateaus at a potential of about 0.4 V; the charge/discharge plateaus correspond to the redox current peaks in the cyclic voltammetry curves. The apparently different slopes of the three electrodes ($k_{MnO_2} < k_{composite} < k_{NiHCF}$) at the beginning of the charge process and subsequent charge/discharge plateaus indicate that both components can develop their respective advantages and lead to higher capacitance in the dual-layer composite structure.[33] Figure 3C shows the energy−power

dx.doi.org/10.1021/am5011173 | ACS Appl. Mater. Interfaces 2014, 6, 6196−6201

plots of the three kinds of electrodes. Because NiHCF and MnO_2 are very different, here, we briefly discussed three different categories of samples: capacitor-type materials (EDLC), battery-type materials (such as NiHCF), and pseudocapacitive materials (such as RuO_2 and MnO_2). It is generally recognized that, for a typical aqueous battery-type material, its energy density is twice that stored in a capacitor-type material charged with the same electric charge to the same voltage.[38,39] Although MnO_2 shows a electrochemical behavior similar to that of capacitor-type materials, however, its inner mechanism of energy storage depends on the fast, reversible redox reactions at the surface, like batteries. Although MnO_2 shows no obvious discharge plateau like NiHCF, in fact, its discharge curve (in Figure 3B) can be regarded as a cohesive whole consist with numerous small discharge plateaus. Therefore, there is no difference between NiHCF and MnO_2 in terms of the energy density calculation. The energy density of the composite electrode is 60.3 Wh kg^{-1} at 1050 W kg^{-1} and remains 36.2 Wh kg^{-1} at 42000 W kg^{-1}, which is much higher than the other two kinds of electrodes, as shown in the energy–power plots (Figure 3C). Such energy and power performances are significantly better than those of the current electrochemical capacitive materials reported recently, such as the energy density of 15.4 Wh kg^{-1} for a MnO_2/GO composite electrode at 1000 Wh kg^{-1} and 32.5 Wh kg^{-1} for a MnO_2-coated carbon nanofiber array core–shell nanostructure at 6216 W kg^{-1}.[20,40,41] Formulas for calculating the power density and energy density of both capacitor-type and battery-type materials are given in the SI, and all of the data were calculated based on the total mass loadings of the active material.

Figure 3D shows the charge/discharge cycling performance evaluated between −0.1 and +0.9 V at a current density of 5 A g^{-1}. The simple NiHCF electrode shows good cycling stability as reported;[26] however, there is still some capacitance fading; about 91.2% of the discharge capacitance in the first cycle was retained after 500 segments. As a comparison, NiHCF@MnO_2 manifests excellent cycling stability; the discharge capacitance shows almost no fading after 500 segments. The excellent cycling stability and rate capability of these NiHCF@MnO_2 electrodes might be attributed to the rational design and engineering of the unique nanostructure and composition. As we all know, for MnO_2, the capacitance fading is very little in the cycling process because ion exchange only happens at a very small surface layer.[1,42] However, for NiHCF, similar to other battery-type materials, redox reactions happen in the inner space, and ion migration may cause the electrode material to be partially dissolved; thus, these types of materials usually exhibit faster capacitance fading. In our unique dual-layer composite structure, MnO_2 sprouts from the conductive acetylene black and grows into a new hierarchical layer covering the whole electrode. The petty local empty space at the interface was protected by the ultrathin platelike subunits and offered a relatively stable ion concentration environment, thus leading to improved stability.

In summary, we have rationally designed and synthesized a hierarchical dual-layer composite structure constructed by an ultrathin platelike MnO_2-coated NiHCF local-area three-dimensional network. This interesting functional nanostructure simultaneously integrates the structural and compositional design rationales for composite cathode materials based on the complementarity of a reticular battery-type MOF structure and a high-power pseudocapacitive MnO_2 layer and the synergy effect (ICE effect) of this kind of dual-layer structure. When evaluated as a cathode material for supercapacitors, the as-prepared NiHCF@MnO_2 electrode manifests enhanced specific capacitance, high energy density, and excellent cycling performance. The manufacture strategy demonstrated here is simple and versatile for the preparation of other dual-layer composite electrodes. What is more, the ICE effect of the dual-layer structure comes to light for the first time with a guidance function for future studies.

■ ASSOCIATED CONTENT

Supporting Information

Experimental details, XRD spectra, BET surface area and pore-size distribution, high-magnification SEM images of the electrode surface, XPS spectra, and CVs at different scan rates. This material is available free of charge via the Internet at http://pubs.acs.org.

■ AUTHOR INFORMATION

Corresponding Author

*E-mail: cqw@ustc.edu.cn.

Notes

The authors declare no competing financial interest.

■ ACKNOWLEDGMENTS

This work was supported by the National Natural Science Foundation (Grants 21271163 and U1232211).

■ REFERENCES

(1) Simon, P.; Gogotsi, Y. Materials for Electrochemical Capacitors. *Nat. Mater.* **2008**, *7*, 845–854.

(2) Qu, Q.; Yang, S.; Feng, X. 2D Sandwich-Like Sheets of Iron Oxide Grown on Graphene as High Energy Anode Material for Supercapacitors. *Adv. Mater.* **2011**, *23*, 5574–5580.

(3) Xu, Y.; Lin, Z.; Huang, X.; Liu, Y.; Huang, Y.; Duan, X. Flexible Solid-State Supercapacitors Based on Three-Dimensional Graphene Hydrogel Films. *ACS Nano* **2013**, *7*, 4042–4049.

(4) Toupin, M.; Brousse, T.; Bélanger, D. Charge Storage Mechanism of MnO_2 Electrode Used in Aqueous Electrochemical Capacitor. *Chem. Mater.* **2004**, *16*, 3184–3190.

(5) Wang, G.; Zhang, L.; Zhang, J. A Review of Electrode Materials for Electrochemical Supercapacitors. *Chem. Soc. Rev.* **2012**, *41*, 797–828.

(6) Yu, G.; Xie, X.; Pan, L.; Bao, Z.; Cui, Y. Hybrid Nanostructured Materials for High-Performance Electrochemical Capacitors. *Nano Energy* **2012**, *2*, 213–234.

(7) Wei, W.; Cui, X.; Chen, W.; Ivey, D. G. Manganese Oxide-Based Materials as Electrochemical Supercapacitor Electrodes. *Chem. Soc. Rev.* **2011**, *40*, 1697–1721.

(8) Pandolfo, A. G.; Hollenkamp, A. F. Carbon Properties and Their Role in Supercapacitors. *J. Power Sources* **2006**, *157*, 11–27.

(9) Fan, Z.; Yan, J.; Wei, T.; Zhi, L.; Ning, G.; Li, T.; Wei, F. Asymmetric Supercapacitors Based on Graphene/MnO_2 and Activated Carbon Nanofiber Electrodes with High Power and Energy Density. *Adv. Funct. Mater.* **2011**, *21*, 2366–2375.

(10) Liu, C.; Yu, Z.; Neff, D.; Zhamu, A.; Jang, B. Z. Graphene-Based Supercapacitor with an Ultrahigh Energy Density. *Nano Lett.* **2010**, *10*, 4863–4868.

(11) Cao, L.; Xu, F.; Liang, Y. Y.; Li, H. L. Preparation of the Novel Nanocomposite $Co(OH)_2$/Ultra-Stable Y Zeolite and Its Application as a Supercapacitor with High Energy Density. *Adv. Mater.* **2004**, *16*, 1853–1857.

(12) Yu, P.; Zhang, X.; Wang, D.; Wang, L.; Ma, Y. Shape-Controlled Synthesis of 3D Hierarchical MnO_2 Nanostructures for Electrochemical Supercapacitors. *Cryst. Growth Des.* **2008**, *9*, 528–533.

(13) Subramanian, V.; Zhu, H.; Vajtai, R.; Ajayan, P.; Wei, B. Hydrothermal Synthesis and Pseudocapacitance Properties of MnO_2 Nanostructures. *J. Phys. Chem. B* **2005**, *109*, 20207−20214.
(14) Jiang, H.; Zhao, T.; Ma, J.; Yan, C.; Li, C. Ultrafine Manganese Dioxide Nanowire Network for High-Performance Supercapacitors. *Chem. Commun.* **2011**, *47*, 1264−1266.
(15) Li, Q.; Wang, Z.-L.; Li, G.-R.; Guo, R.; Ding, L.-X.; Tong, Y.-X. Design and Synthesis of MnO_2/Mn/MnO_2 Sandwich-Structured Nanotube Arrays with High Supercapacitive Performance for Electrochemical Energy Storage. *Nano Lett.* **2012**, *12*, 3803−3807.
(16) Yu, G.; Hu, L.; Liu, N.; Wang, H.; Vosgueritchian, M.; Yang, Y.; Cui, Y.; Bao, Z. Enhancing the Supercapacitor Performance of Graphene/MnO_2 Nanostructured Electrodes by Conductive Wrapping. *Nano Lett.* **2011**, *11*, 4438−4442.
(17) Hu, L.; Chen, W.; Xie, X.; Liu, N.; Yang, Y.; Wu, H.; Yao, Y.; Pasta, M.; Alshareef, H. N.; Cui, Y. Symmetrical MnO_2−Carbon Nanotube−Textile Nanostructures for Wearable Pseudocapacitors with High Mass Loading. *ACS Nano* **2011**, *5*, 8904−8913.
(18) Zhang, H.; Cao, G.; Wang, Z.; Yang, Y.; Shi, Z.; Gu, Z. Growth of Manganese Oxide Nanoflowers on Vertically-Aligned Carbon Nanotube Arrays for High-Rate Electrochemical Capacitive Energy Storage. *Nano Lett.* **2008**, *8*, 2664−2668.
(19) Dong, S.; Chen, X.; Gu, L.; Zhou, X.; Li, L.; Liu, Z.; Han, P.; Xu, H.; Yao, J.; Wang, H. One Dimensional MnO_2/Titanium Nitride Nanotube Coaxial Arrays for High Performance Electrochemical Capacitive Energy Storage. *Energy Environ. Sci.* **2011**, *4*, 3502−3508.
(20) Chen, S.; Zhu, J.; Wu, X.; Han, Q.; Wang, X. Graphene Oxide−MnO_2 Nanocomposites for Supercapacitors. *ACS Nano* **2010**, *4*, 2822−2830.
(21) Zhang, F.; Zhang, T.; Yang, X.; Zhang, L.; Leng, K.; Huang, Y.; Chen, Y. A High-Performance Supercapacitor−Battery Hybrid Energy Storage Device Based on Graphene-Enhanced Electrode Materials with Ultrahigh Energy Density. *Energy Environ. Sci.* **2013**, *6*, 1623−1632.
(22) Pell, W. G.; Conway, B. E. Peculiarities and Requirements of Asymmetric Capacitor Devices Based on Combination of Capacitor and Battery-Type Electrodes. *J. Power Sources* **2004**, *136*, 334−345.
(23) Rowsell, J. L.; Yaghi, O. M. Strategies for Hydrogen Storage in Metal−Organic Frameworks. *Angew. Chem., Int. Ed.* **2005**, *44*, 4670−4679.
(24) Wessells, C. D.; Huggins, R. A.; Cui, Y. Copper Hexacyanoferrate Battery Electrodes with Long Cycle Life and High Power. *Nat. Commun.* **2011**, *2*, 550.
(25) Chen, J.; Huang, K.; Liu, S.; Hu, X. Electrochemical Supercapacitor Behavior of $Ni_3(Fe(CN)_6)_2(H_2O)$ Nanoparticles. *J. Power Sources* **2009**, *186*, 565−569.
(26) Wessells, C. D.; Peddada, S. V.; Huggins, R. A.; Cui, Y. Nickel Hexacyanoferrate Nanoparticle Electrodes for Aqueous Sodium and Potassium Ion Batteries. *Nano Lett.* **2011**, *11*, 5421−5425.
(27) Pang, S. C.; Anderson, M. A.; Chapman, T. W. Novel Electrode Materials for Thin-Film Ultracapacitors: Comparison of Electrochemical Properties of Sol−Gel-Derived and Electrodeposited Manganese Dioxide. *J. Electrochem. Soc.* **2000**, *147*, 444−450.
(28) Wei, W.; Cui, X.; Chen, W.; Ivey, D. G. Phase-Controlled Synthesis of MnO_2 Nanocrystals by Anodic Electrodeposition: Implications for High-Rate Capability Electrochemical Supercapacitors. *J. Phys. Chem. C* **2008**, *112*, 15075−15083.
(29) Xue, L.; Hao, H.; Wei, Z.; Huang, T.; Yu, A. A Hierarchical Porous MnO_2-Based Electrode for Electrochemical Capacitor. *J. Solid State Electrochem.* **2011**, *15*, 485−491.
(30) Buser, H.; Schwarzenbach, D.; Petter, W.; Ludi, A. The Crystal Structure of Prussian Blue: $Fe_4[Fe(CN)_6]_3{\cdot}xH_2O$. *Inorg. Chem.* **1977**, *16*, 2704−2710.
(31) Herren, F.; Fischer, P.; Ludi, A.; Hälg, W. Neutron Diffraction Study of Prussian Blue, $Fe_4[Fe(CN)_6]_3{\cdot}xH_2O$. Location of Water Molecules and Long-Range Magnetic Order. *Inorg. Chem.* **1980**, *19*, 956−959.
(32) Chigane, M.; Ishikawa, M. Manganese Oxide Thin Film Preparation by Potentiostatic Electrolyses and Electrochromism. *J. Electrochem. Soc.* **2000**, *147*, 2246−2251.
(33) Wang, Y.; Zhong, H.; Hu, L.; Yan, N.; Hu, H.; Chen, Q. Manganese Hexacyanoferrate/MnO_2 Composite Nanostructures as a Cathode Material for Supercapacitors. *J. Mater. Chem. A* **2013**, *1*, 2621−2630.
(34) Gosser, D. K. *Cyclic Voltammetry: Simulation and Analysis of Reaction Mechanisms*; VCH: New York, 1993; pp 37−42.
(35) Kissinger, P. T.; Heineman, W. R. Cyclic Voltammetry. *J. Chem. Educ.* **1983**, *60*, 702.
(36) Jiang, H.; Yang, L.; Li, C.; Yan, C.; Lee, P. S.; Ma, J. High-Rate Electrochemical Capacitors from Highly Graphitic Carbon-Tipped Manganese Oxide/Mesoporous Carbon/Manganese Oxide Hybrid Nanowires. *Energy Environ. Sci.* **2011**, *4*, 1813−1819.
(37) Chen, L. F.; Huang, Z. H.; Liang, H. W.; Guan, Q. F.; Yu, S. H. Bacterial-Cellulose-Derived Carbon Nanofiber@MnO_2 and Nitrogen-Doped Carbon Nanofiber Electrode Materials: An Asymmetric Supercapacitor with High Energy and Power Density. *Adv. Mater.* **2013**, *25*, 4746−4752.
(38) Conway, B. E. Transition from "Supercapacitor" to "Battery" Behavior in Electrochemical Energy Storage. *J. Electrochem. Soc.* **1991**, *138*, 1539−1548.
(39) Conway, B. *Electrochemical Supercapacitors: Scientific Fundamentals and Technological Applications (POD)*; Kluwer Academic/Plenum: New York, 1999; pp 20−31.
(40) Chen, Z.; Qin, Y.; Weng, D.; Xiao, Q.; Peng, Y.; Wang, X.; Li, H.; Wei, F.; Lu, Y. Design and Synthesis of Hierarchical Nanowire Composites for Electrochemical Energy Storage. *Adv. Funct. Mater.* **2009**, *19*, 3420−3426.
(41) Liu, J.; Essner, J.; Li, J. Hybrid Supercapacitor Based on Coaxially Coated Manganese Oxide on Vertically Aligned Carbon Nanofiber Arrays. *Chem. Mater.* **2010**, *22*, 5022−5030.
(42) Kang, J.; Hirata, A.; Kang, L.; Zhang, X.; Hou, Y.; Chen, L.; Li, C.; Fujita, T.; Akagi, K.; Chen, M. Enhanced Supercapacitor Performance of MnO_2 by Atomic Doping. *Angew. Chem.* **2013**, *125*, 1708−1711.